North Atlantic Oscillation dynamics recorded in central Norwegian fjord sediments during the past 2800 years

Johan C. Faust[a, b, *], Karl Fabian[a], Gesa Milzer[d], Jacques Giraudeau[d], Jochen Knies[a]

[a] Geological Survey of Norway, 7491 Trondheim, Norway
[b] University of Tromsø, Department of Geology, 9011 Tromsø, Norway
[d] Universite Bordeaux 1 UMR CNRS 5805 EPOC, 33405 Talence cedex , France

*Corresponding author: Norges geologiske undersøkelse /Geological Survey of Norway (NGU), Marine Geology, Postboks 6315 Sluppen, 7491 Trondheim, Norway. Tel.: +47 7390 4000. E-mail address: Johan.Faust@ngu.no

The North Atlantic Oscillation (NAO) is the leading mode of atmospheric circulation variability in the North Atlantic region[1]. Along the Norwegian coast it has a strong impact on precipitation, temperature and wind intensity changes, thereby affecting energy supply and demand, fisheries, agricultural, marine and terrestrial ecological dynamics[2-4]. Long term NAO reconstructions are crucial to better understand NAO variability in its response to climate forcing factors, and assess predictability and possible shifts associated with on-going global warming. However, existing records are rare and often inconsistent[5]. By comparing geochemical measurements with instrumental data we show that primary productivity recorded in central Norwegian fjord sediments is sensitive to NAO variability. This observation is used to calibrate paleoproductivity changes to a 500-year reconstruction of winter NAO[6] and to establish a high resolution NAO proxy record covering the past 2800 years. We find that NAO variability coincides with climatically associated changes in paleodemographics and Northern Hemisphere (NH) glacier advances. Furthermore, a strong volcanic eruption may have induced the onset of the Little Ice Age (LIA), which is marked by a rapid transition from a stable positive to a stable negative NAO phase.

Apart from the northward flowing North Atlantic Current (NAC), the climate in northern Europe is strongly influenced by the North Atlantic Oscillation (NAO)[1,7,8]. This dominant mode of atmospheric circulation is most pronounced during winter (Dec-Mar) and swings between two phases: a positive (negative) NAO generates periods of warmer and wetter (colder and dryer) climate conditions in north-western Europe[9].

Instrumental time series are too short to reveal NAO responses to internal and external climate forcing with confidence. Paleo-NAO records based on historical records, tree ring or ice core data are shorter than ~950 years[10], and have large uncertainties for the pre-industrial period[5,8,11]. General challenges for NAO reconstructions are its possible non-stationarity, and its strong alteration on very short time scales requiring high resolution (winter) paleoclimatic records. Only the latter can provide the essential knowledge for NAO prediction and quantification of possible anthropogenic changes.

The Norwegian coastal area is supposed to be consistently influenced by NAO variability over long time scales[8]. General high sedimentation in Norwegian fjords, together with the possibility to quantify environmental parameters such as water exchange and freshwater input, offer an excellent opportunity for studying local responses to short-term variability in the Earth's climate. Here we use the geochemical record of two sediment cores: the upper five meter of the piston core MD99-2292[12], and multi-core MC99-3 (hereafter referred to as MC99). They were recovered from the Trondheimsfjord, central Norway (Fig. S1, supplementary information), and have a temporal resolution of 1.8-3 years covering the past 2800 years.

The most important factors regulating primary productivity in fjords are light, temperature, wind-driven vertical mixing and freshwater runoff i.e. nutrient supply (e.g. Fe, N, P)[13-15].

Thus, the strong impact of the NAO on changes on physical climate parameters, such as wind, temperature and precipitation in Norway, influences ecological dynamics in marine and terrestrial systems and encompasses change in (e.g.) the phytoplankton production in terms of timing of reproduction and population dynamics[2,3,16]. In particular, the annual spring bloom, most likely the strongest primary productivity event in fjords, is triggered by the strength of spring river discharge due to snow melt[14,15]. During this period autotrophic production and heterotrophic consumption are uncoupled, resulting in dense phytoplankton population and large amounts of aggregated particles reaching the seafloor,[17] nourishing the benthic population[2].

Principle component analysis (PCA) indicates that for the last 50 years the three climate components of 1) winter-spring (DJFMAM) river discharge (R), 2) winter (DJFM) air temperature (T), and 3) precipitation (P) from the Trondheimsfjord area are strongly related. The first principal component (PCA1) explains 81 % of the variance (supplementary information, Tab. S3), and combines the three physical factors into a new RTP index (Fig. 1). The concurrent changes of the three climate components in the Trondheimsfjord region appear to be caused by changes in the large-scale atmospheric climate pattern as defined through the winter NAO index[1] (supplementary information, Fig. S4).

In accordance with investigations of Trondheimsfjord surface sediments[18] a strong connection ($r^2 = 0.8$) between marine derived organic matter and $CaCO_3$ retrieved from the short sediment core MC99 indicates carbonate marine productivity to be the main $CaCO_3$ source in Trondheimsfjord sediments during the past 50 years (supplementary information Fig. S2). Moreover, $CaCO_3$ variations are closely linked to the RTP index (Fig. 1 and S3), implying that the combined impact of air temperature, precipitation and river discharge on marine productivity is directly reflected by the $CaCO_3$ concentrations in Trondheimsfjord sediments. Due to the insufficient resolution of the sediment record the available number of $CaCO_3$ measurements does not allow a reliable statistical comparison with the instrumental time series although, the $CaCO_3$ record from MC99 closely follows the winter NAO variation during the past fifty years. Temporal offsets between relative maxima and minima lie within chronological uncertainties (Fig. 1). Accordingly, winter NAO apparently is very well recorded by $CaCO_3$ in Trondheimsfjord sediments due to its impact on the annual spring bloom intensity, suggesting planktic and benthic carbonate productivity during spring as a promising proxy for NAO reconstruction.

In the sediment core MD99-2292, $CaCO_3$ percentages coincide closely with its high resolution (1.8 - 3.0 years) Ca/Si record (Fig. S5). This enables us to compare Ca/Si to reliable[11] winter (DJF) NAO reconstructions based on early instrumental and documentary proxy data covering the past 500 years (AD 1500-1990)[6]. A correlation of $r^2 = 0.8$ between Ca/Si and an averaged winter NAO index was achieved by adapting the depth-age relation of Ca/Si within its 1-sigma age error range to the Luterbacher [6] NAO using a dynamic time-warping algorithm (Fig. 2 and supplementary information). The derived linear calibration function was used to calculate a winter NAO_{TRD} proxy index for the past 2800 years (Fig. 3).

As previously proposed[10], but so far not completely recorded, the NAO_{TRD} reveals persistent positive values during the Medieval Climate Anomaly (MCA, ~950 to ~1250 A.D.)[19]. A rapid change towards a stable negative mode occurs at the LIA[20] onset followed by a much more variable behavior during the past 300 years. The only previous NAO reconstruction beyond 1000 A.D. (NAO_{PCA3})[21] suggests a similar overall paleo-NAO pattern (Fig. 3). However, the NAO_{TRD} varies more and does not contain the NAO_{PCA3} extended stable periods between e.g. ~500 to ~350 B.C. and ~0 to ~200 A.D. In particular the longest persistent NAO_{PCA3} period (1100 - 1400 A.D.), originating from the calibration of the NAO_{PCA3}[10,21], differs from our record. The differences between the proxies are probably related to different response times of the proxies, dating uncertainties, and maybe also to changes in the stationarity of the NAO spatial pattern[8]. Nevertheless, spectral analysis of NAO_{TRD} reveals dominant periodicities of about 300 (±20), 170 (±10) and 66 (±2) years (Fig. S7, supplementary information), which are consistent with the cyclicities of the NAO_{PCA3}[21]. The occurrence of a 300-year climatic cycle, identified in NH meteorological observations and terrestrial climate archives, historically has been related to changes in solar activity[22,23], but to our knowledge this has not been confirmed. Although there might be an intrinsic atmospheric (NAO) periodicity driven by external forcing, the apparent 300-year cycle could also be a spurious periodicity of a red-noise climate process (Fig. S7, supplementary information).

It is noteworthy that climatically associated changes in central European paleo-demographics[24] coincide with long and short term NAO_{TRD} variations (Fig. 3 and Tab. S4). Socio-economic crises, population migration, and settlement desertion intensified during negative NAO_{TRD} phases while positive NAO_{TRD} phases seem to heighten sustained demographic and economic growths. Moreover, a pronounced negative NAO_{TRD} overlaps with the collapse of the Classical Maya Civilization (~800 to ~1000 A.D.)[25] during an annual precipitation reduction of 40 %[25] in Mexico that is assumed to be caused by a shift of the Intertropical Convergence Zone (ITCZ)[26]. Within the same period glaciers advanced in Canada and Iceland[20] (Fig.3) as well as in the Alps, Alaska and Tibet[27]. The synchronicity of the central-American precipitation anomaly and widespread glacier advance in the NH suggest a common forcing promoting a negative NAO phase.

It is notable that transitions from positive to negative phases of the NAO_{TRD} are often rapid, whilst the increases back to positive values are more gradual. Possibly the spontaneous phase changes are related to threshold transitions triggered by internal or external forcing. For example, distinct positive to negative NAO_{TRD} shifts with subsequent advance of NH glaciers[20,27] occurred at the same time as the two major volcanic eruptions of the past 2800 years (536 and 1257 A.D.[20,28,29]) (Fig. 3). The rapid NAO_{TRD} MCA-LIA transition in the mid to late 13th century differs from the NAO reconstruction based on tree rings and speleothems (NAO_{ms}[10], Fig. 3), but is consistent with ice-cap development reconstructed in Canada[20] (Fig. 3). Associated climate modeling shows that volcanic-induced cooler climate conditions can continue after the aerosols are removed by sea-ice/ocean feedbacks over long time scales[20]. This scenario could explain the long negative NAO_{TRD} phase from 1250-1450 A.D.. Furthermore, periods of "volcanic-solar downturns"[30] seem to correspond with negative NAO_{TRD} phases (Fig. 3). Nevertheless, many phase changes in the NAO_{TRD} record are unaffected by volcanic activity, and other forcing factors such as internal atmospheric dynamical processes[31] may be responsible for NAO variability.

Compared to other paleoclimate records the LIA onset occurs relatively early in the NAO_{TRD}. We propose that this difference reflects different response times between the ocean and the atmosphere to internal or external forcing on short time scales. A positive NAO, as during the MCA, is generally associated with stronger eastward air-flow towards northern Europe supporting a strengthening of the North Atlantic Current (NAC) and Meridional Overturning Circulation[32]. The rapid NAO reversal at ~1250 A.D. may have decreased heat and moisture transport towards northern latitudes, whilst the buffering effect of the ocean may have prevented an immediate temperature drop in northern Europe. By following Miller [20], we propose that the onset of the LIA occurred around 1250 A.D. when volcanic activity triggered large changes in the atmospheric circulation. A delayed LIA appearance by 100 years or so and a slower MCA-LIA transition in other records[30] is likely the result of the delayed response of the oceanic circulation to atmospheric forcing. Similar scenarios may also hold true for other periods of rapid NAO_{TRD} shifts.

The here presented first high-resolution winter NAO reconstruction from marine sediments (Fig. 3) reveals a strong connection between NH climate history and NAO regional impact in central Norway. Persistent positive and negative NAO phases are in accordance with cooler and warmer climate periods during the late Holocene, such as MCA and LIA. Rapid phase transitions related to large volcanic eruptions indicate the existence of internal atmospheric thresholds and instabilities in the atmospheric circulation pattern. Ongoing climate change and global warming requires improved physical modeling of the NAO to gain better knowledge of the feedback mechanisms involved in these changes to answer the important questions of which processes are potential triggers, and which are the main amplifiers of large scale climatic changes. Compared to the historic NAO variability over the last 300-400 years, the NAO_{TRD} proxy record shows comparable amplitudes over the last 2800 years, but also indicates that positive and negative phases are typically more persistent.

Material and Methods

The data presented here were obtained from two sediment cores, MD99-2292 and MC99, recovered at the same site in the Trondheimsfjord Seaward Basin (Fig. S1). The 31 m long sediment core MD99-2292 (water depth 486 m, 63°28'62"N, 10°11'63"E) was taken by the research vessel “Marion Dufresne” in 1999. Prior to sediment sampling the elemental composition of the first five meters were measured in 0.5 cm steps using an Avaatech X-ray fluorescence (XRF) core scanner. Additional X-ray images using the SCOPIX system were taken at EPOC, CNRS/University of Bordeaux 1, France. Subsequently sediment slices (1 cm deep, 1.5 cm wide, 7 cm long) were taken in 4 cm intervals. The short (26 cm) multicore MC99 (5.5 cm diameter) was collected by the research vessel “Seisma” in April 2011 (water depth 504 m, 63°28'37"N, 10°11'37"E). The core was sliced in 1 cm intervals aboard the research vessel, and samples were stored in plastic bags at -18°C. Prior to further analyses, all samples (MD99-2292 and MC99) were freeze-dried and, except for grain size measurements, homogenised through gentle grinding.

Total carbon (TC) and total organic carbon (C_{org}) measurements were performed at the Geological Survey of Norway (NGU). C_{org} and TC were determined with a LECO SC-444. Prior to the C_{org} analysis, sediment subsamples (ca. 200 mg) were treated with 10 % (vol.) hydrochloric acid at 60°C, and subsequently washed 10 times with distilled water to remove inorganic carbon (carbonate). Carbonate content was calculated as $CaCO_3$ = (TC- C_{org}) x 8.33.

Total nitrogen (N_{tot} in wt%) was determined using an elemental analyzer isotope ratio mass spectrometer (EA-IRMS) at EPOC, CNRS/University of Bordeaux 1, France. The inorganic nitrogen (N_{inorg}) content was analysed on 20 mg sediment subsamples treated with KOBr-KOH solution to remove organic nitrogen (see Knies [33] for details) using an EA-IRMS (Iso-Analytical Ltd., UK). The organic proportion of the total nitrogen content was calculated by subtracting the N_{inorg} fraction from N_{tot}. Stable carbon isotopes of the C_{org} fraction ($\delta^{13}C_{org}$) were measured on decarbonated (10 % HCl) aliquots using an EA-IRMS (Iso-Analytical Ltd., UK). $\delta^{13}C_{org}$ values are given in per mil vs. Vienna-PDB.

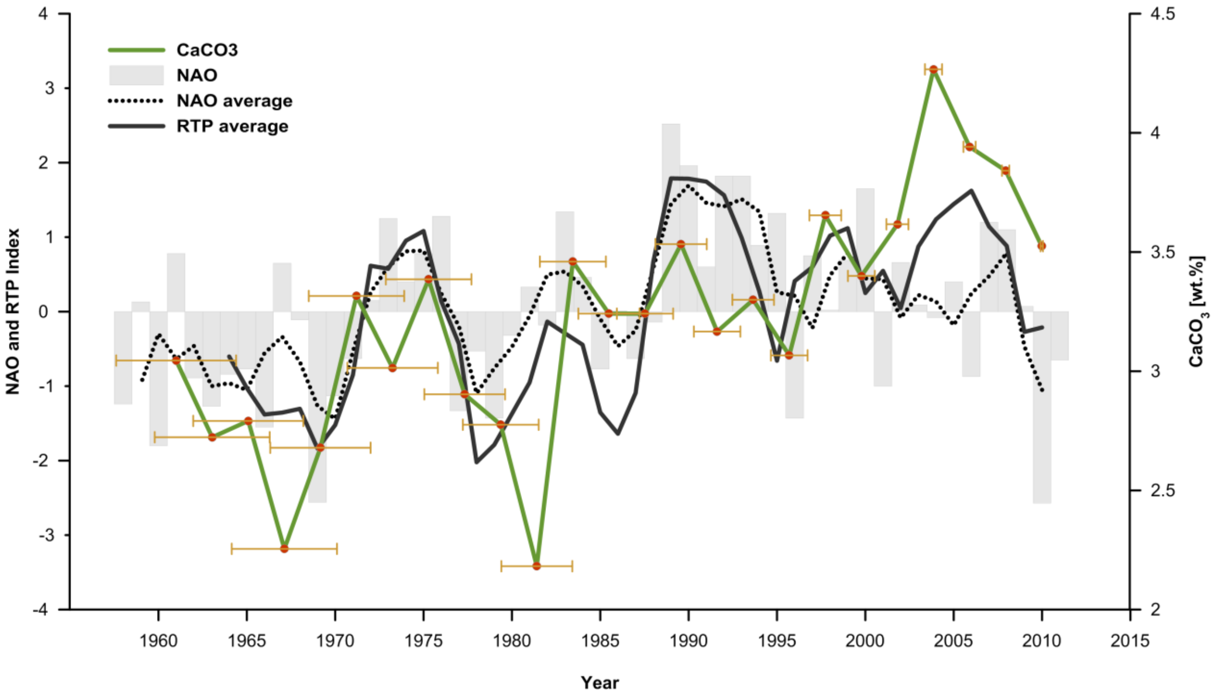

Figure 1: Comparison of instrumental data with $CaCO_3$ over the past 50 years. 3 point running average of RTP index (black line) combines instrumental records of winter-spring (DJFMAM) river discharge (R), winter (DJFM) air temperature (T) and precipitation (P) from the Trondheimsfjord area since 1963 (supplementary information). Grey bars are the annual winter NAO index[1] and dotted line is a 3 point running average. $CaCO_3$ concentration from MC99 (green line) follows the course of the averaged instrumental data in the range of the dating error (yellow bars).

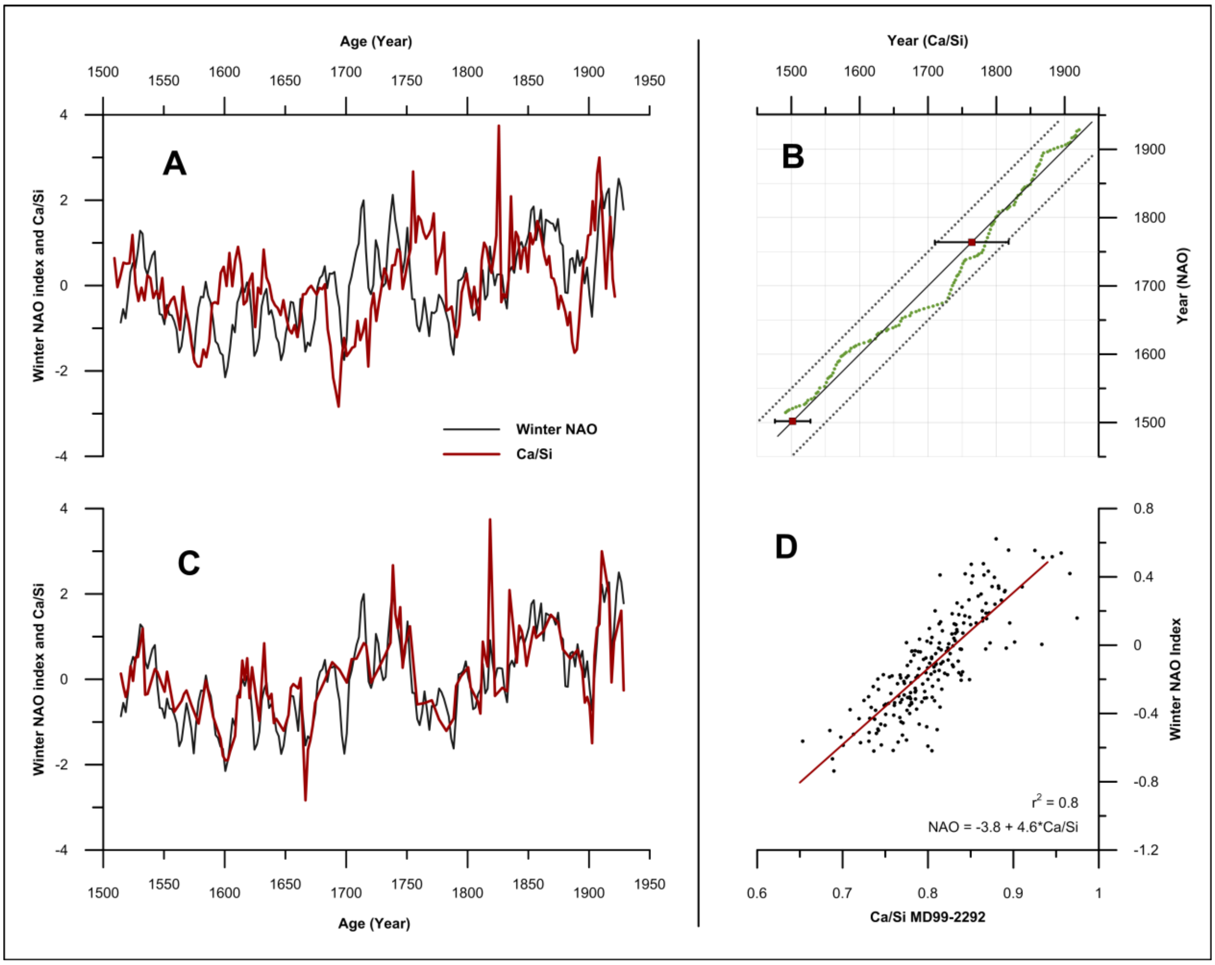

Figure 2: NAO_{TRD} calibration using a DTW fit A) Comparison between Ca/Si (MD99-2292) and averaged winter NAO index.[6] B) DTW fit between Ca/Si and averaged winter NAO index[6]. Red squares indicate ^{14}C ages (MD99-2292) with age error sigma 1 (Tab. S1). Dotted lines indicate ±50 year deviation. C) DTW fitted Ca/Si and averaged winter NAO index[6]. D) Calibration curve (r^2 = 0.8) based on Ca/Si winter NAO in C).

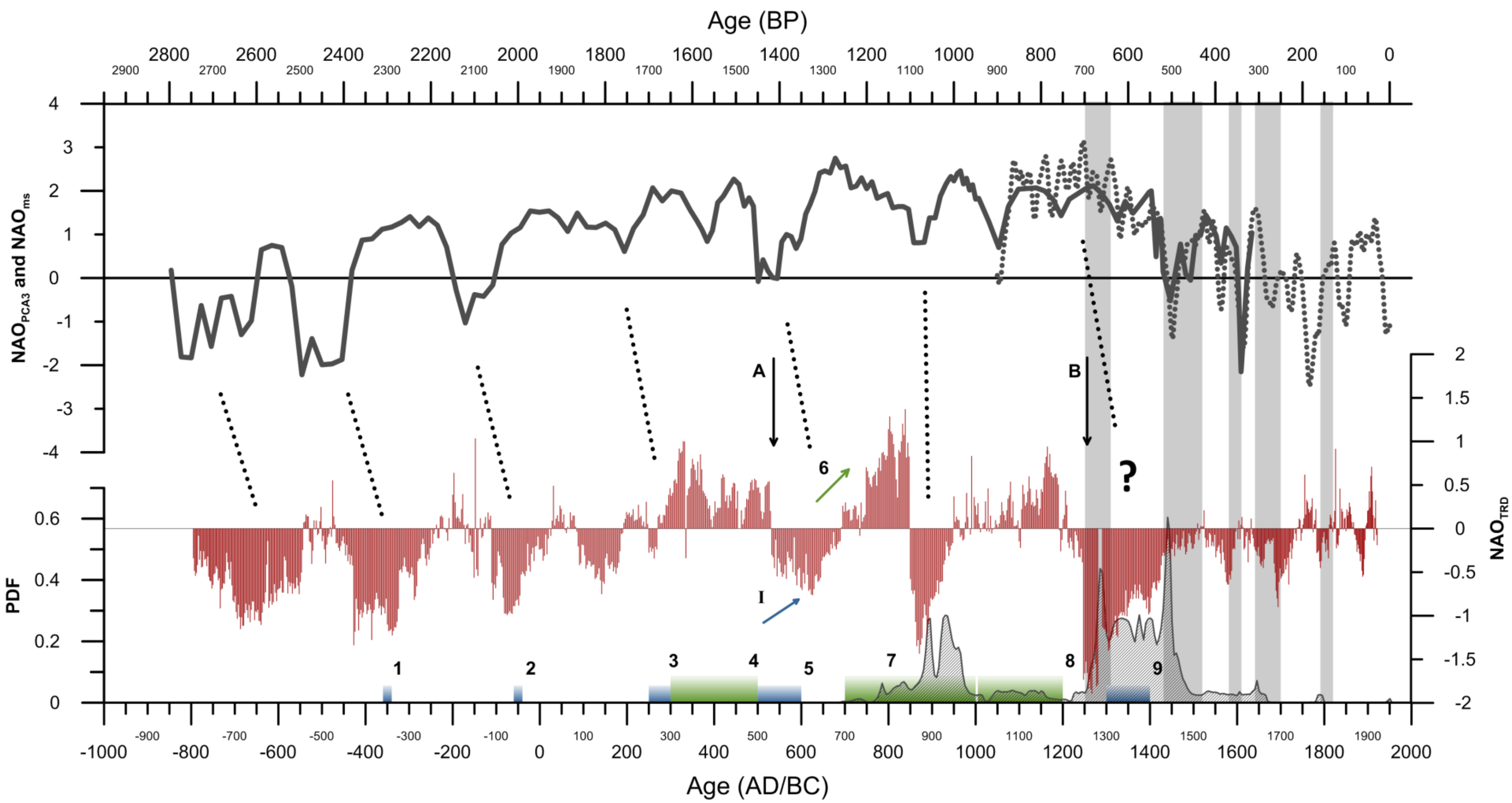

Fig. 3: Comparison between NAO_{TRD} and NH paleo-climate records. Longest NAO reconstruction (NAO_{PCA3})[21] available to date (black line) calibrated on a NAO record based on tree ring and speleothems (NAO_{ms})[10] (dotted black line). Black arrows: major volcanic eruptions in A) 536 A.D.[28] and B) 1257 A.D.[29]. European paleo-demographic climatic associated development[24] (Tab. S4) indicated by: blue squares (political turmoil, culture change, population instability) and green arrow/squares (demographic expansion, economic prosperity). Filled grey plot: ice cap expansion in Arctic Canada as probability density functions (PDF) of snow line depression[20]. Blue arrow (I) NH glacier advances during the 6th century[27]. Vertical grey bars: Periods of "Volcanic-Solar downturns" as defined by Pages 2k [30].

Acknowledgments

For their interest, stimulating discussions and many useful comments we thank our colleagues Simone Sauer and Benjamin Snook. This work is a contribution to the CASE Initial Training Network funded by the European Community's 7th Framework Programme FP7 2007/2013, Marie-Curie Actions, under Grant Agreement No. 238111.

References

1. Hurrell JW. Decadal Trends in the North-Atlantic Oscillation - Regional Temperatures and Precipitation. *Science* 1995, **269**(5224)**:** 676-679.
2. Drinkwater KF, Belgrano A, Borja A, Conversi A, Edwards M, Greene CH*, et al.* the response of marine ecosystems to climate variability associated with the North Atlantic Oscillation. *The North Atlantic Oscillation: Climatic Significance and Environmental Impact*, vol. 134. AGU: Washington, DC, 2003, pp 211-234.
3. Ottersen G, Planque B, Belgrano A, Post E, Reid P, Stenseth N. Ecological effects of the North Atlantic Oscillation. *Oecologia* 2001, **128**(1)**:** 1-14.
4. Hurrell JW, Kushnir Y, Ottersen G, Visbeck M. *The North Atlantic Oscillation: climatic significance and environmental impact*, vol. 134. American Geophysical Union, 2003.
5. Pinto JG, Raible CC. Past and recent changes in the North Atlantic oscillation. *Wires Clim Change* 2012, **3**(1)**:** 79-90.
6. Luterbacher J, Xoplaki E, Dietrich D, Jones PD, Davies TD, Portis D*, et al.* Extending North Atlantic Oscillation reconstructions back to 1500. *Atmos Sci Lett* 2001, **2**(1-4)**:** 114-124.
7. Nesje A, Lie Ø, Dahl SO. Is the North Atlantic Oscillation reflected in Scandinavian glacier mass balance records? *Journal of Quaternary Science* 2000, **15**(6)**:** 587-601.
8. Lehner F, Raible CC, Stocker TF. Testing the robustness of a precipitation proxy-based North Atlantic Oscillation reconstruction. *Quaternary Sci Rev* 2012, **45:** 85-94.
9. Wanner H, Brönnimann S, Casty C, Gyalistras D, Luterbacher J, Schmutz C*, et al.* North Atlantic Oscillation – Concepts And Studies. *Surveys in Geophysics* 2001, **22**(4)**:** 321-381.
10. Trouet V, Esper J, Graham NE, Baker A, Scourse JD, Frank DC. Persistent Positive North Atlantic Oscillation Mode Dominated the Medieval Climate Anomaly. *Science* 2009, **324**(5923)**:** 78-80.
11. Schmutz C, Luterbacher J, Gyalistras D, Xoplaki E, Wanner H. Can we trust proxy-based NAO index reconstructions? *Geophys Res Lett* 2000, **27**(8)**:** 1135-1138.
12. Bøe R, Rise L, Blikra LH, Longva O, Eide A. Holocene mass-movement processes in Trondheimsfjorden, Central Norway. *Norw J Geol* 2003, **83**(1)**:** 3-22.
13. Wassmann P, Svendsen H, Keck A, Reigstad M. Selected aspects of the physical oceanography and particle fluxes in fjords of northern Norway. *Journal of Marine Systems* 1996, **8**(1–2)**:** 53-71.
14. Öztürk M, Steinnes E, Sakshaug E. Iron speciation in the Trondheim fjord from the perspective of iron limitation for phytoplankton. *Estuar Coast Shelf S* 2002, **55**(2)**:** 197-212.
15. Sakshaug E, Myklestad S. Studies on the phytoplankton ecology of the trondheimsfjord. III. Dynamics of phytoplankton blooms in relation to environmental factors, bioassay experiments and parameters for the physiological state of the populations. *Journal of Experimental Marine Biology and Ecology* 1973, **11**(2)**:** 157-188.
16. Belgrano A, Lindahl O, Hernroth B. North Atlantic Oscillation primary productivity and toxic phytoplankton in the Gullmar Fjord, Sweden (1985-1996). *P Roy Soc B-Biol Sci* 1999, **266**(1418)**:** 425-430.
17. Kristiansen S, Farbrot T, Naustvoll LJ. Spring bloom nutrient dynamics in the Oslofjord. *Mar Ecol Prog Ser* 2001, **219:** 41-49.

18. Faust JC, Knies J, Slagstad T, Vogt C, Milzer G, Girausdeau J. Geochemical composition of Trondheimsfjord surface sediments: Sources and spatial variability of marine and terrigenous components. *Cont Shelf Res* Paper I.
19. Mann ME, Zhang ZH, Rutherford S, Bradley RS, Hughes MK, Shindell D*, et al.* Global Signatures and Dynamical Origins of the Little Ice Age and Medieval Climate Anomaly. *Science* 2009, **326**(5957)**:** 1256-1260.
20. Miller GH, Geirsdottir A, Zhong YF, Larsen DJ, Otto-Bliesner BL, Holland MM*, et al.* Abrupt onset of the Little Ice Age triggered by volcanism and sustained by sea-ice/ocean feedbacks. *Geophys Res Lett* 2012, **39**.
21. Olsen J, Anderson NJ, Knudsen MF. Variability of the North Atlantic Oscillation over the past 5,200 years. *Nat Geosci* 2012, **5**(11)**:** 808-812.
22. Clough H. Synchronous variations in solar and terrestrial phenomena. *The Astrophysical Journal* 1905, **22:** 42.
23. Kingsmill T. A 300-Year Climatic and Solar Cycle. *Nature* 1906, **73:** 413-414.
24. Büntgen U, Tegel W, Nicolussi K, McCormick M, Frank D, Trouet V*, et al.* 2500 Years of European Climate Variability and Human Susceptibility. *Science* 2011, **331**(6017)**:** 578-582.
25. Medina-Elizalde M, Rohling EJ. Collapse of Classic Maya Civilization Related to Modest Reduction in Precipitation. *Science* 2012, **335**(6071)**:** 956-959.
26. Haug GH, Gunther D, Peterson LC, Sigman DM, Hughen KA, Aeschlimann B. Climate and the collapse of Maya civilization. *Science* 2003, **299**(5613)**:** 1731-1735.
27. Wanner H, Beer J, Butikofer J, Crowley TJ, Cubasch U, Fluckiger J*, et al.* Mid- to Late Holocene climate change: an overview. *Quaternary Sci Rev* 2008, **27**(19-20)**:** 1791-1828.
28. Larsen LB, Vinther BM, Briffa KR, Melvin TM, Clausen HB, Jones PD*, et al.* New ice core evidence for a volcanic cause of the AD 536 dust veil. *Geophys Res Lett* 2008, **35**(4).
29. Lavigne F, Degeai JP, Komorowski JC, Guillet S, Robert V, Lahitte P*, et al.* Source of the great A.D. 1257 mystery eruption unveiled, Samalas volcano, Rinjani Volcanic Complex, Indonesia. *P Natl Acad Sci USA* 2013, **110**(42)**:** 16742-16747.
30. Pages 2k C. Continental-scale temperature variability during the past two millennia. *Nat Geosci* 2013, **6**(6)**:** 339.
31. Jung T, Vitart F, Ferranti L, Morcrette JJ. Origin and predictability of the extreme negative NAO winter of 2009/10. *Geophys Res Lett* 2011, **38**.
32. Trouet V, Scourse JD, Raible CC. North Atlantic storminess and Atlantic Meridional Overturning Circulation during the last Millennium: Reconciling contradictory proxy records of NAO variability. *Global Planet Change* 2012, **84-85:** 48-55.
33. Knies J, Brookes S, Schubert CJ. Re-assessing the nitrogen signal in continental margin sediments: New insights from the high northern latitudes. *Earth Planet Sc Lett* 2007, **253**(3-4)**:** 471-484.

Supplementary Paper III

Study area

The temperate Trondheimsfjord is located in the central part of Norway (Fig. S1) and, with a length of approximately 135 km, it is the third longest fjord in the country[2]. Three sills (the Agdenes Sill at the entrance (max. 330 m water depth), the Tautra Ridge in the middle section (max. 100 m water depth) and the Skarnsund in the inner part (max. water depth 100 m)) divide the Trondheimsfjord into four main basins: Stjørnfjord, Seaward basin, Middle fjord and Beistadfjord (Fig. S1) (for detailed maps of bathymetry and topography of the drainage area, we refer to http://kart.statkart.no). The average tide in the Trondheimsfjord is 1.8 m, the average water depth is 165 m and the maximum water depth (620 m) is found at the mouth of the Seaward basin [3].

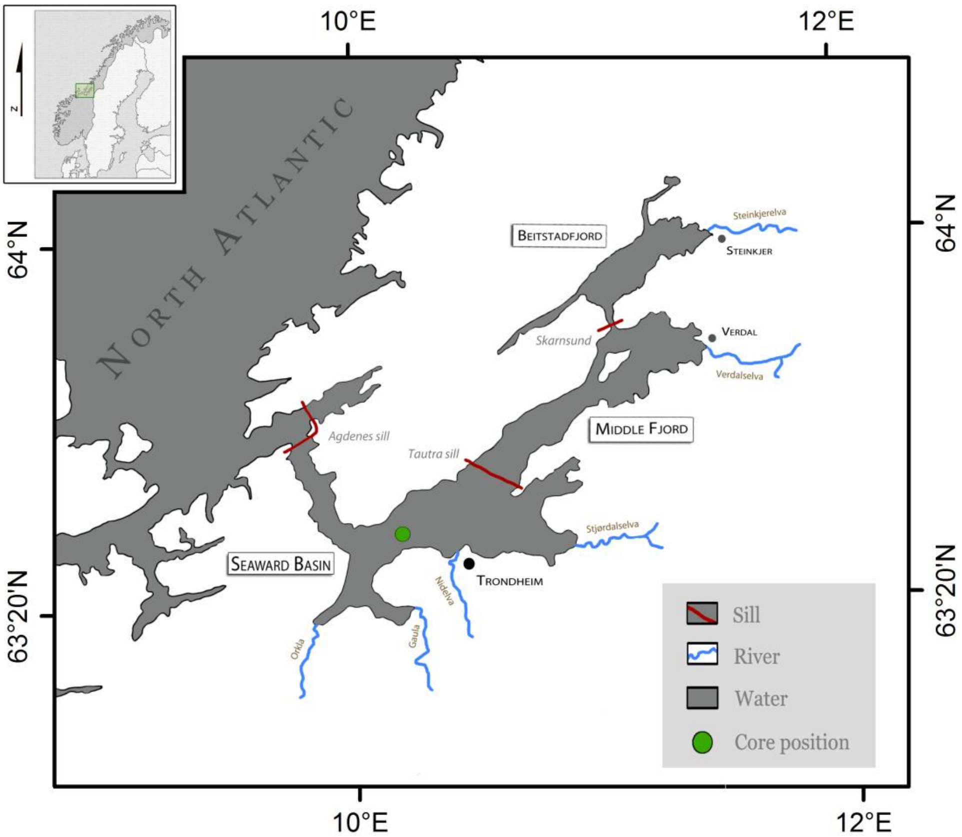

Figure S1: A) Location of the study area (upper left corner) and map of the Trondheimsfjord with the position of the sediment core MD99-2292 and MC99 (green circle). Three sills divide the fjord into three main basins and the six main rivers enter the fjord from the south-east.

Origin of organic matter

On the basis of sixty evenly distributed surface sediment samples around the entire Trondheimsfjord an index for the variable input of marine versus terrigenous organic matter (MT index) was generated by Faust et al (Paper I): MT index = 16.68 – 0.034 * F_{terr} + 0.65 * $\delta^{13}C_{org}$. F_{terr} is the fraction of terrestrial organic carbon, which is calculated from the N_{org}/C_{org} ratio[4]. To calculate F_{terr}, the lowest and highest N_{org}/C_{org} ratios (0.052 and 0.113) revealed from the surface sediment analysis (Faust et al Paper I) were used to define the marine and terrestrial end members, respectively. Thus, MT index variations (Fig. S2) in the sedimentary record discussed in this study is tied to the modern environmental conditions in the fjord and positive (negative) MT index values indicate higher (lower) marine organic matter input.

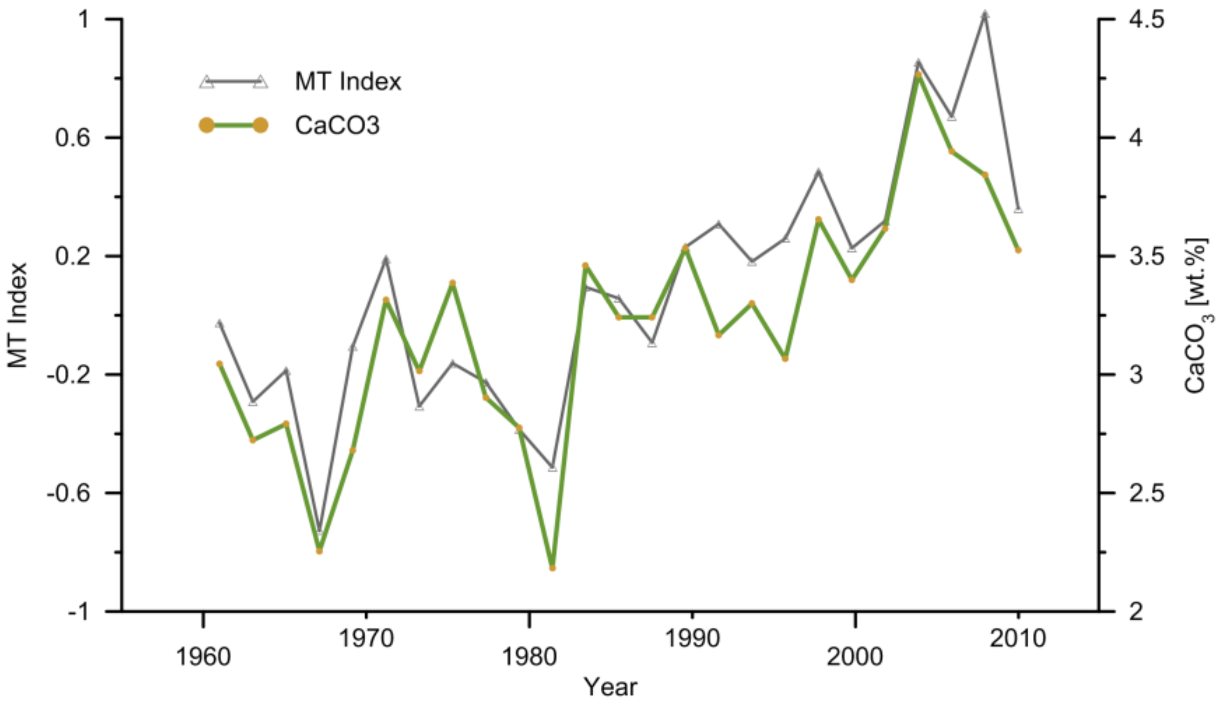

Figure S2: A strong connection between positive (negative) MT index values indicate higher (lower) marine organic matter input and $CaCO_3$ retrieved from the short sediment core MC99 indicates carbonate marine productivity to be the main $CaCO_3$ source in Trondheimsfjord sediments during the past 50 years.

Instrumental Data: NAO versus temperature, precipitation and river discharge

Seasonal and annual mean air temperature and precipitation records for the Trondheimsfjord region since 1900 were obtained from the Norwegian Meteorological Institute (www.eklima.no). Time series (1963-present) of river discharge for the six largest rivers entering the Trondheimsfjord, Gaula, Orkla, Nidelva, Stjørdalselva, Verdalselva and Steinkjerelva (Fig. S1) were obtained from the Norwegian Water Resource and Energy Directorate (www.nve.no). All data were collected at monitoring stations close to river outlets. The winter (December – March) PC-based NAO index[5] is based on the difference of normalised sea level pressure between Lisbon, Portugal and Stykkishomur, Iceland and the dataset was retrieved from https://climatedataguide.ucar.edu/climate-data/hurrell-north-atlantic-oscillation-nao-index-pc-based. Annual precipitation and river discharge into the Trondheimsfjord are strongly correlated[3]. However, the highest runoff occurs in late April to May and is primarily caused by snow melt (winter precipitation). As winter-spring river runoff, winter temperature and winter precipitation are closely linked to each other 81 % of the variance is explained by score of the first axis of principal component analysis (Tab. S3).

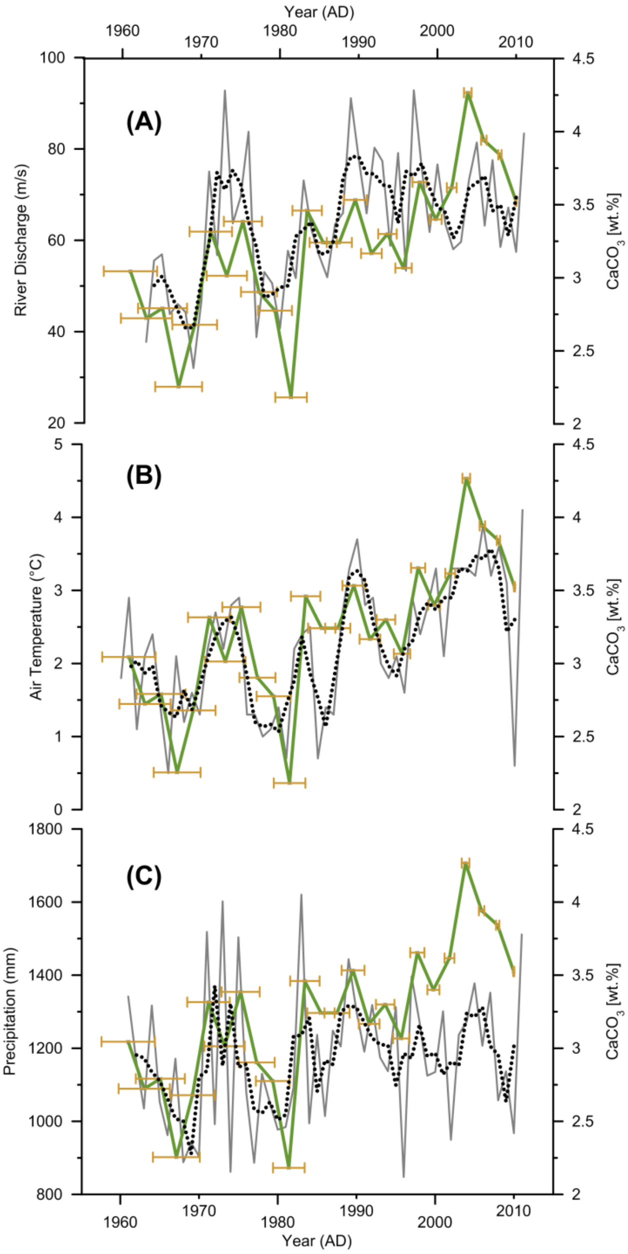

Figure S3: $CaCO_3$ from the sediment core MC99 compared to Trondheimsfjord regional variations of A) winter-spring (DJFMAM) river discharge B) winter (DJFM) air temperature and C) winter (DJFM) precipitation. Dotted black line is a 3 point running average.

Our Trondheimsfjord regional RTP record (PCA1) shows a very good correlation to the winter NAO index ($r^2 = 0.6$, Fig. S4), confirming that regional temperature and precipitation in the Trondheimsfjord area are responding to changes in large-scale Northern Hemisphere climate patterns.

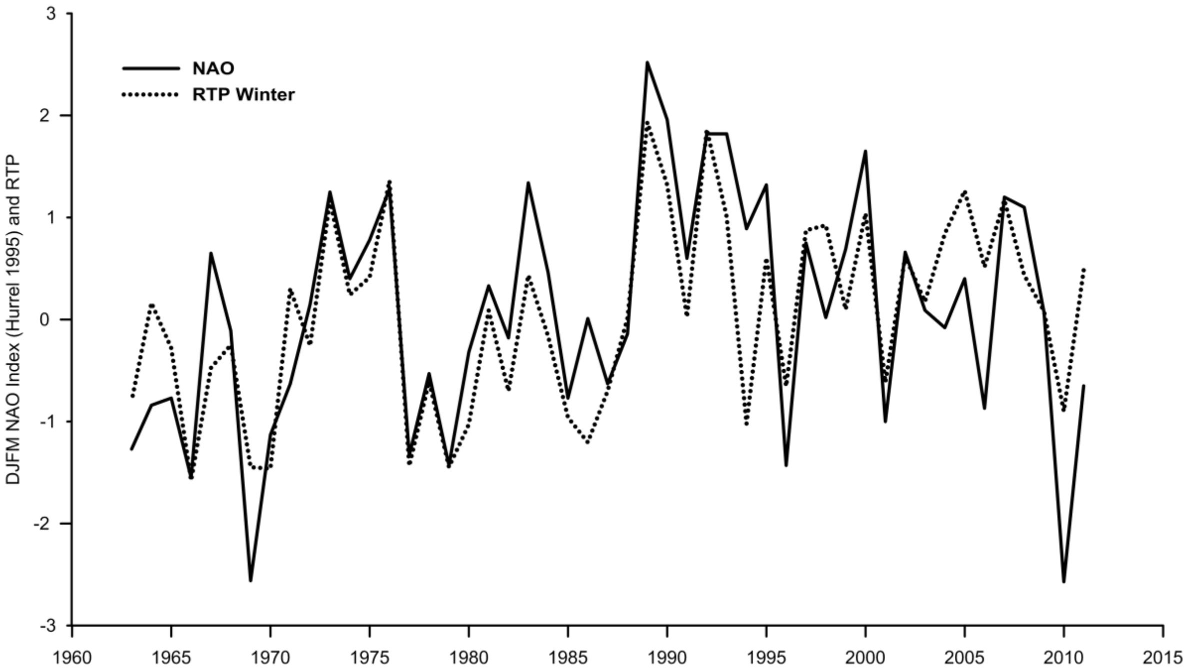

Figure S4: Winter NAO index[5] versus RTP index since 1963.

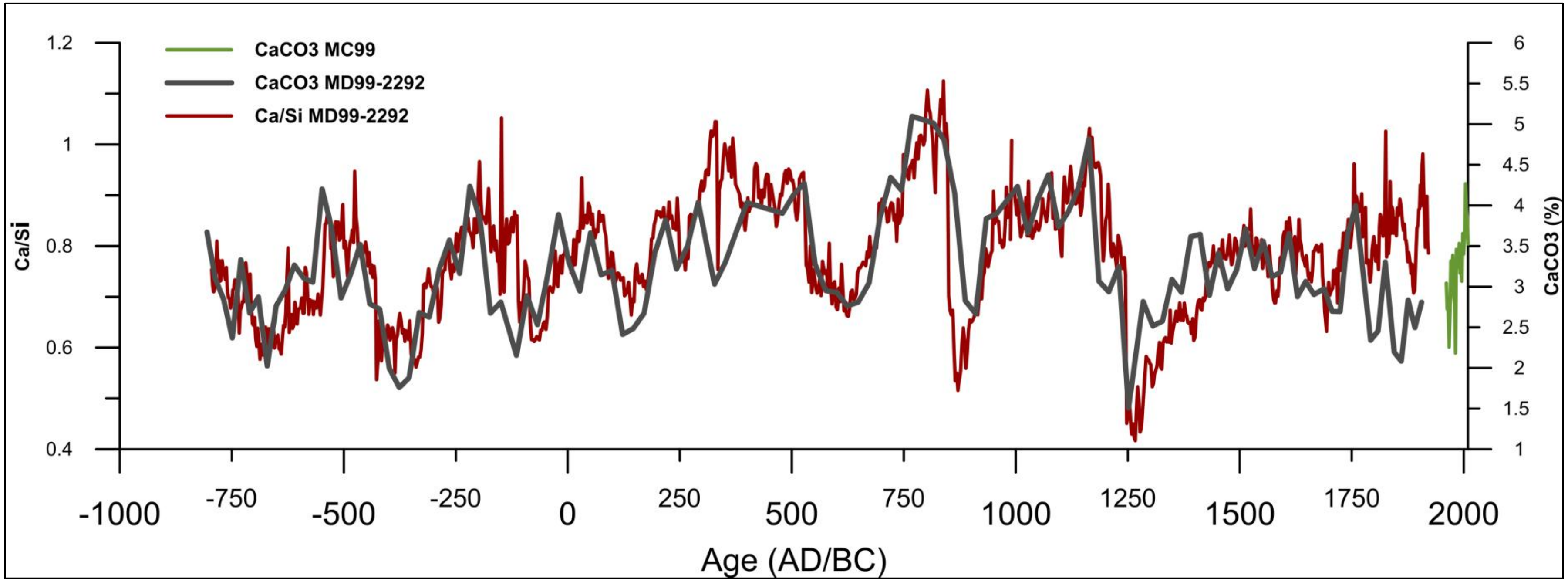

Figure S5: $CaCO_3$ in the gravity core MD99-2292 is in correspondence with $CaCO_3$ variations in the MC99. The ultra high resolution Ca/Si record closely resembles the $CaCO_3$ percentage in the MD99-2292.

NAO_{TRD} calibration

To convert Ca/Si ratios from MD99-2292 to estimates of the winter NAO index for the last 2800 years, the upper part (containing about 200 measurements between 1500 and 1930 A.D.) was fitted to a smoothed version of the winter NAO index of Luterbacher [1].

The smoothing kernel used,

$$\mathrm{Ker}(L,t) := \begin{cases} \max\left(0, 1-\frac{t}{2}\right), & t \geq 0 \\ \exp\left(\frac{2L}{t}\right), & t \leq 0 \end{cases}$$

takes into account both exponential mixing during sedimentation and linear averaging of the XRF sensor over its footprint area. Its only free parameter, the exponential decay constant, was chosen such that the variability of the smoothed record best resembled the Ca/Si variability (Fig. S6).

Because MD99-2292 contains only two ^{14}C ages in the time interval 1500 to 1930 A.D., its interpolated age model was modified to achieve an optimal fit of the Ca/Si signal to the smoothed winter NAO index, while keeping the dated sediment layers within their 1 sigma error range. This was performed using a dynamic time-warping (DTW) algorithm as described by Hofmann [6] and results in the transfer function between the two time scales shown in Fig. 2B. The suggested fit (Fig. 2C) shows that after alignment the two standardized signals agree very well, although near 1700 A.D. there is an alternative signal alignment. After alignment, the original Ca/Si measurement is plotted against the matching smoothed NAO index value of Luterbacher [1] in Fig. 2D. A robust linear fit (neglecting 10% of the data points furthest away from an initial fit) results in a clear ($r^2 = 0.8$) linear relation, whereby

$$smoothed\ NAO = 4.6\frac{Ca}{Si} - 3.8$$

The fit quality related to all data points is $r^2 = 0.7$. This relation was used to calibrate the Ca/Si record from MD99-2292 over the full time interval of 2,800 years.

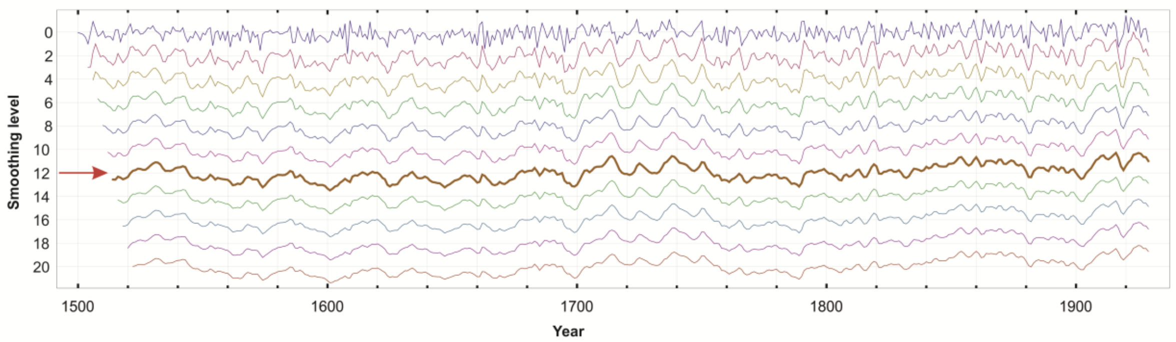

Figure S6: Smoothing of the NAO index[1] required to correctly account for delays in the transport and sedimentary deposition processes, as well as averaging during measurement, due to the finite overlapping footprints of the XRF sensor. Above) Original record (0) and increasingly smoothed versions (2-20) of the NAO index[1]. Right) Smoothing kernel (12) visually chosen to represent the high-frequency reduction observed in the Ca/Si record from the MD99-2292. Note that Ca/Si signal can only serve as a proxy for an accordingly smoothed NAO index.

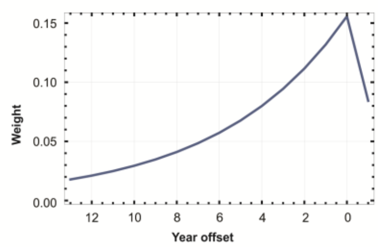

Spectral Analysis

The Ca/Si record from the sediment core MD99-2292 was analyzed for periodicities using Fourier transforms of length 512 with Welch overlapping windows (WOSA, overlap 384). The WOSA periodogram shows spectral peaks at frequencies corresponding to about 300 ±20, 170 ±10 and 66 ±2 years (Fig. S7). None of these peaks is statistically significant as a climatic periodicity. To confirm this we created random sequences $(r_n)_{n=1\ldots1002}$ of AR(1) processes based on white noise $(w_n)_{n=1\ldots1002}$ with standard deviation $\sigma = 0.45$ according to $r_0 = 0$, $\rho=0.92$, and

$$r_{n+1} = \rho\, r_n + w_n.$$

These sequences were smoothed by the same smoothing kernel as used for the NAO data and finally analyzed by the WOSA periodogram[7]. While the average periodogram corresponds to the known theoretical red noise spectrum each individual random record shows distinct peaks at varying frequencies. Within the first 50 trials we already found a spectrum closely resembling the one obtained from the observed Ca/Si record.

It is therefore impossible to relate the observed periodicities to true eigenfrequencies of the climate system. Yet, because they originate from the NAO signal, these frequencies may be observed in other related time series covering the same time interval even if they are spurious.

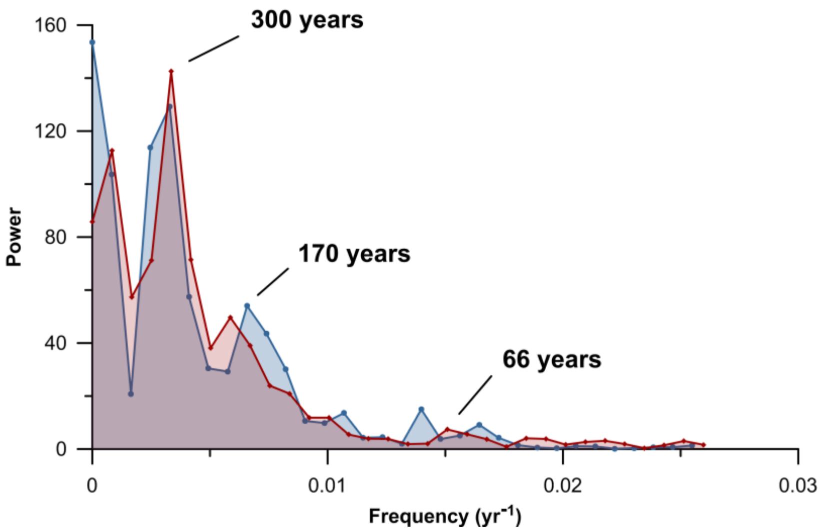

Figure S7: One out of 50 random AR(1) processes (blue) shows a WOSA periodogram similar to the observed signal (red).

Chronology

The chronology of the core MC99 is based on ^{210}Pb and ^{137}Cs content on neighbouring sediment core in the multi-corer rack (MC99-1). ^{210}Pb and ^{137}Cs measurements were made at EPOC, CNRS/University of Bordeaux 1, France. According to the age model of Milzer [8] (Fig. S8), the sedimentation rate of the MC99-1 is 0.49 cm/year and the core base age is 1959. The dating error increases gradually down core from ±0.07 to ±3.53 years.

The age model of the upper five meters of the MD99-2292[9] is based on eight ^{14}C-AMS dates and polynomial regression between these dates (Fig. S8). The ^{14}C-AMS dates were determined on shell material at the Leibniz Laboratory (University of Kiel, Germany) and at the Laboratoire de Mesure du Carbone 14 (Gif sur Yvette Cedex, France) (Tab. S1). We applied a reservoir correction of 400 years (ΔR = 0) and converted the radiocarbon dates into calibrated years with the Calib 6.0.1 software[10]. Six sand layers between 3-8 cm thick in various core depths (Tab. S2) were identified as gravitational mass movement and therefore as short term sedimentation events. The depth of the six slides (in total 35 cm) were subtracted from the total core depth prior to the construction of the age model.

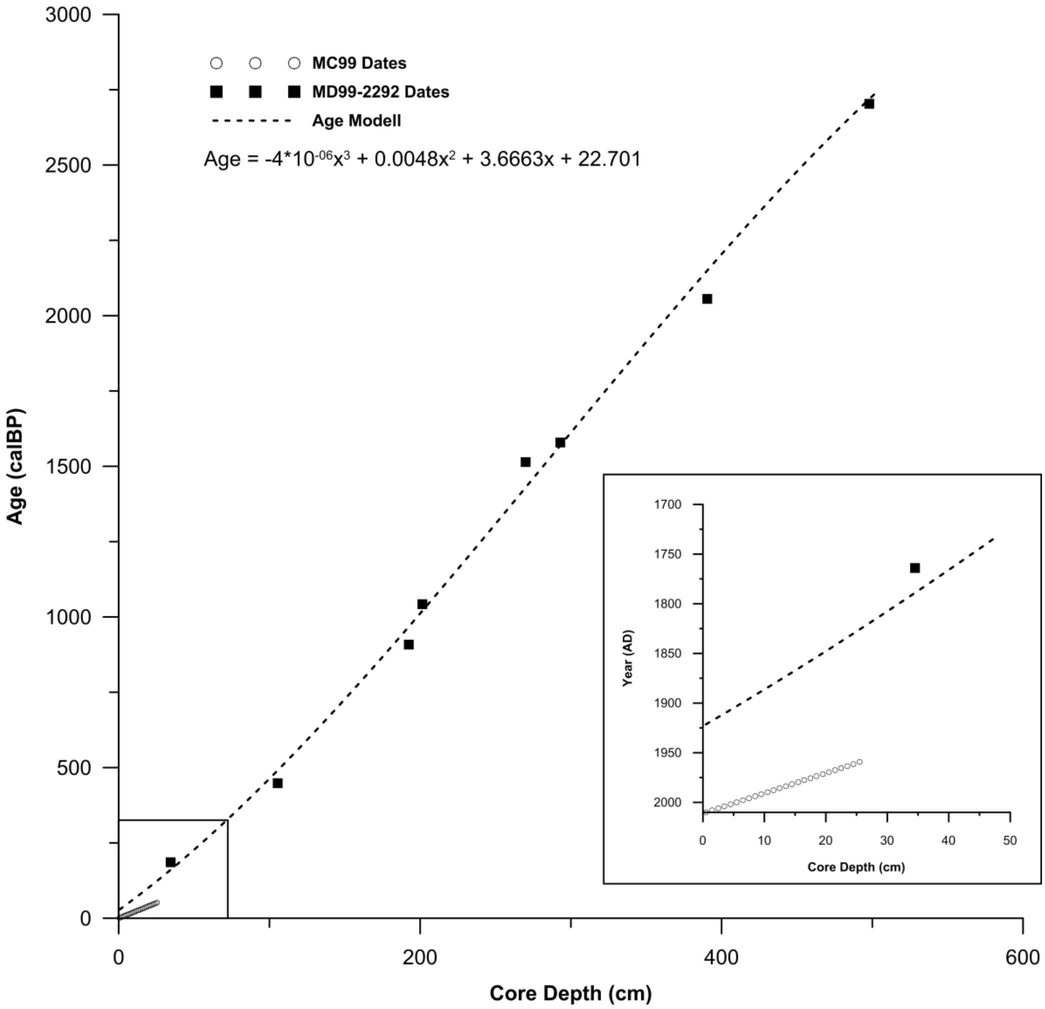

Figure S8: Age model for the MD99-2292. Black squares represent calibrated ^{14}C dates from core MD99-2292 and open circles are ^{210}Pb dates from core MC99[8]. Dashed line represents the age model for the MD99-2292. Equation of the 3rd order polynomial regression is shown at the upper left side. The inlayed graph on the lower right side is the magnification of the past~300 years marked by the square at the lower left corner.

References

1. Luterbacher J, Xoplaki E, Dietrich D, Jones PD, Davies TD, Portis D*, et al.* Extending North Atlantic Oscillation reconstructions back to 1500. *Atmos Sci Lett* 2001, **2**(1-4)**:** 114-124.
2. Jacobson P. Physical oceanography of the Trondheimsfjord. *Geophysical & Astrophysical Fluid Dynamics* 1983, **26**(1-2)**:** 3-26.
3. Sakshaug E, Sneli J-A. *Trondheimsfjorden*. Tapir Forlag: Trondheim, 2000.
4. Perdue EM, Koprivnjak JF. Using the C/N ratio to estimate terrigenous inputs of organic matter to aquatic environments. *Estuar Coast Shelf S* 2007, **73**(1-2)**:** 65-72.
5. Hurrell JW. Decadal Trends in the North-Atlantic Oscillation - Regional Temperatures and Precipitation. *Science* 1995, **269**(5224)**:** 676-679.
6. Hofmann DI, Fabian K, Schmieder F, Donner B, Bleil U. A stratigraphic network across the Subtropical Front in the central South Atlantic: Multi-parameter correlation of magnetic susceptibility, density, X-ray fluorescence and delta O-18 records. *Earth Planet Sc Lett* 2005, **240**(3-4)**:** 694-709.
7. Percival DB. *Spectral analysis for physical applications*. Cambridge University Press, 1993.
8. Milzer G, Giraudeau J, Schmidt S, Eynaud F, Faust J. Qualitative and quantitative reconstruction of surface water characteristics and recent hydrographic changes in the Trondheimsfjord, central Norway. *Clim Past Discuss* 2013, **9**(4)**:** 4553-4598.
9. Bøe R, Rise L, Blikra LH, Longva O, Eide A. Holocene mass-movement processes in Trondheimsfjorden, Central Norway. *Norw J Geol* 2003, **83**(1)**:** 3-22.
10. Stuiver M, Reimer PJ. Extended 14C data base and revised CALIB 3.0 14C age calibration program. *Radiocarbon* 1993, **35**(1)**:** 215-230.
11. Büntgen U, Tegel W, Nicolussi K, McCormick M, Frank D, Trouet V*, et al.* 2500 Years of European Climate Variability and Human Susceptibility. *Science* 2011, **331**(6017)**:** 578-582.

Table S1: Chronological information

Core	Depth [cmbsf]	Lab code [a)]	Material	^{14}C Age BP (uncorrected)	Model Age [BP] [b)]	Sedimentation rate (cm/a)
MD99-2292	34.5	SacA23876	Shell fragment	550±35	186±54	0.2
MD99-2292	105.5	KIA-38731	Shell (Modiolaria)	800±25	448±26	0.2
MD99-2292	192.5	SacA 19110	Shell fragment	1360±30	908±36	0.2
MD99-2292	201.5	SacA23879	Shell fragment	1495±30	1042±50	0.2
MD99-2292	270	KIA-38732	Shell (Abra alba)	1960±25	1514±43.5	0.2
MD99-2292	293	SacA 19111	Shell fragment	2015±30	1579±46	0.2
MD99-2292	390.5	SacA 19112	Shell fragment	2420±30	2056±49	0.2
MD99-2292	498	KIA-38734	Shell fragment	2915±35	2703±32	0.2

[a)] KIA: Leibniz Laboratory (University of Kiel, Germany); SacA: Laboratoire de Mesure du Carbone 14 (Gif sur Yvette Cedex, France)
[b)] Ages with 1 sigma range were determined using Calib 6.0.1[10]

Table S2: Depth of six slides subtracted from the total core depth

Slide Number	Core Depth	Slide Length (cm)
1	23-26	3
2	40-44	4
3	67-70	3
4	157-165	8
5	305-310	5
6	326-332	6
7	407-413	6

Table S3: PCA Analysis

			Loadings		
	Eigenvalue	Variance (%)	R[DJFMAM][a)]	T[DJFM][b)]	P[DJFM][c)]
PCA1	2.44	81.2	0.92	0.71	0.97
PCA2	0.37	12.3	0.4	0.18	-0.24
PCA3	0.19	6.5	0	0.69	0

[a)] River discharge (m/s)
[b)] Temperature (°C)
[c)] Precipitation (mm)

Table S4: European paleo-demographic climatic associated development shown in Fig. 3. All data are from Büntgen [11]

Number in Fig. 3	Period	Histroical Event	Climate summer conditions
1	~350 B.C.	Celtic Expansion, followed by the Late Iron Age	Colder Temperatures
2	~50 B.C.	Roman Conquest followed by the Roman Empire	Colder Temperatures
3	250-300 A.D.	Crisis in the West Roman Empire marked by barbarian invasion	Distinct drier conditions
4	300-500 A.D.	Dynasties of Constantine and Valentinian	Relative stable conditions
5	500-600 A.D.	Frequent epidemics, disrupt food production of agrarian societies	Sharp drop in precipitation in the first half of the 6th century, NH cooling
6	End 600 - 800 A.D.	Societal consolidation of new kingdoms that developed in the former West Roman Empire	Increase in temperature and precipitation
7	700-1000 A.D.	Sustained demographic growth in the northwest European countryside, establishment of colonies in Iceland and Greenland	Stable wet and warm conditions
8	1000-1200 A.D.	Peak medieval demographic and economic growth	Stable wet and warm conditions
9	1300-1400 A.D.	Widespread famine across central Europe, desertion of Greenland settlements	Colder Temperatures

Table S5: Ca/Si values from the MD99-2292 and calculated NAO$_{TRD}$

Age AD/BC	Ca/Si	NAO$_{TRD}$	Age AD/BC	Ca/Si	NAO$_{TRD}$	Age AD/BC	Ca/Si	NAO$_{TRD}$	Age AD/BC	Ca/Si	NAO$_{TRD}$
1921	0.79	-0.19	1764	0.88	0.23	1583	0.71	-0.53	1382	0.66	-0.76
1920	0.81	-0.07	1762	0.89	0.30	1580	0.69	-0.64	1379	0.67	-0.74
1918	0.90	0.33	1760	0.90	0.33	1578	0.69	-0.64	1376	0.69	-0.64
1916	0.85	0.12	1757	0.86	0.16	1575	0.69	-0.61	1374	0.65	-0.80
1914	0.80	-0.14	1755	0.96	0.62	1573	0.72	-0.50	1371	0.67	-0.71
1912	0.86	0.15	1753	0.85	0.12	1571	0.75	-0.36	1368	0.65	-0.80
1910	0.92	0.43	1751	0.84	0.05	1568	0.77	-0.27	1366	0.69	-0.64
1909	0.98	0.71	1749	0.82	-0.05	1566	0.80	-0.13	1363	0.66	-0.75
1907	0.96	0.60	1747	0.80	-0.14	1563	0.74	-0.40	1361	0.65	-0.81
1905	0.88	0.24	1745	0.85	0.10	1561	0.77	-0.28	1358	0.67	-0.72
1903	0.92	0.43	1742	0.85	0.12	1558	0.79	-0.19	1355	0.65	-0.80
1901	0.87	0.21	1740	0.83	0.02	1556	0.78	-0.21	1353	0.64	-0.85
1899	0.87	0.20	1738	0.83	0.01	1554	0.77	-0.26	1350	0.63	-0.91
1898	0.84	0.06	1736	0.80	-0.14	1551	0.76	-0.33	1347	0.61	-1.01
1896	0.84	0.04	1734	0.82	-0.06	1549	0.81	-0.07	1345	0.67	-0.71
1894	0.80	-0.13	1731	0.83	-0.01	1546	0.78	-0.20	1342	0.61	-1.00
1892	0.75	-0.35	1729	0.80	-0.12	1544	0.79	-0.15	1339	0.62	-0.96
1890	0.71	-0.53	1727	0.78	-0.23	1541	0.78	-0.20	1337	0.61	-1.00
1888	0.71	-0.55	1725	0.75	-0.35	1539	0.81	-0.07	1334	0.62	-0.96
1886	0.72	-0.48	1723	0.79	-0.17	1536	0.82	-0.05	1331	0.62	-0.98
1884	0.76	-0.29	1721	0.77	-0.27	1534	0.78	-0.21	1329	0.61	-1.00
1883	0.75	-0.37	1718	0.69	-0.64	1532	0.80	-0.13	1326	0.56	-1.24
1881	0.76	-0.29	1716	0.75	-0.33	1529	0.78	-0.22	1323	0.56	-1.22
1879	0.78	-0.23	1714	0.74	-0.42	1527	0.80	-0.11	1321	0.61	-1.00
1877	0.79	-0.18	1712	0.73	-0.47	1524	0.87	0.21	1318	0.59	-1.08
1875	0.77	-0.27	1710	0.75	-0.35	1522	0.83	0.03	1315	0.56	-1.21
1873	0.80	-0.13	1707	0.72	-0.51	1519	0.83	0.02	1313	0.56	-1.25
1871	0.81	-0.07	1705	0.71	-0.52	1517	0.83	0.03	1310	0.55	-1.28
1869	0.81	-0.07	1703	0.71	-0.55	1514	0.82	-0.06	1307	0.53	-1.37
1867	0.84	0.07	1701	0.70	-0.57	1512	0.80	-0.13	1305	0.52	-1.40
1865	0.83	0.02	1698	0.73	-0.46	1509	0.84	0.06	1302	0.57	-1.20
1863	0.84	0.08	1696	0.69	-0.61	1507	0.82	-0.03	1299	0.57	-1.19
1861	0.86	0.17	1694	0.63	-0.90	1504	0.81	-0.06	1296	0.58	-1.16
1859	0.88	0.25	1692	0.65	-0.80	1502	0.79	-0.18	1294	0.58	-1.15
1858	0.89	0.30	1689	0.67	-0.71	1499	0.78	-0.23	1291	0.58	-1.13
1856	0.87	0.19	1687	0.72	-0.51	1497	0.78	-0.23	1280	0.44	-1.78
1854	0.86	0.15	1685	0.74	-0.40	1494	0.79	-0.16	1278	0.43	-1.81
1852	0.88	0.22	1683	0.80	-0.11	1492	0.81	-0.08	1275	0.49	-1.55
1850	0.82	-0.03	1680	0.80	-0.14	1489	0.82	-0.05	1272	0.52	-1.40
1848	0.86	0.13	1678	0.80	-0.13	1487	0.79	-0.17	1269	0.48	-1.61
1846	0.85	0.11	1676	0.79	-0.18	1484	0.77	-0.27	1267	0.42	-1.89
1844	0.83	-0.01	1674	0.80	-0.15	1482	0.76	-0.30	1264	0.43	-1.84
1842	0.87	0.20	1671	0.80	-0.12	1479	0.78	-0.21	1261	0.45	-1.74
1840	0.88	0.23	1669	0.80	-0.14	1477	0.82	-0.03	1259	0.43	-1.83
1838	0.83	-0.01	1667	0.79	-0.17	1474	0.80	-0.12	1256	0.47	-1.66
1836	0.93	0.46	1665	0.79	-0.17	1472	0.78	-0.20	1253	0.50	-1.53
1834	0.81	-0.08	1662	0.75	-0.35	1469	0.77	-0.25	1250	0.47	-1.66
1832	0.79	-0.19	1660	0.73	-0.45	1467	0.78	-0.22	1248	0.45	-1.73
1830	0.79	-0.17	1658	0.75	-0.37	1464	0.78	-0.24	1245	0.74	-0.39
1828	0.78	-0.23	1655	0.73	-0.43	1462	0.81	-0.07	1242	0.78	-0.23
1826	1.03	0.92	1653	0.74	-0.40	1459	0.79	-0.17	1239	0.76	-0.33
1824	0.87	0.21	1651	0.76	-0.32	1456	0.76	-0.31	1237	0.76	-0.32
1822	0.84	0.08	1648	0.78	-0.21	1454	0.79	-0.16	1234	0.80	-0.14
1820	0.82	-0.04	1646	0.76	-0.31	1451	0.78	-0.24	1231	0.81	-0.08
1818	0.83	0.03	1644	0.77	-0.26	1449	0.78	-0.23	1228	0.82	-0.03
1816	0.85	0.13	1642	0.77	-0.24	1446	0.75	-0.35	1226	0.75	-0.34
1814	0.86	0.16	1639	0.78	-0.21	1444	0.77	-0.28	1223	0.77	-0.24
1812	0.84	0.05	1637	0.80	-0.11	1441	0.80	-0.12	1220	0.80	-0.15
1810	0.75	-0.34	1635	0.81	-0.07	1439	0.78	-0.23	1217	0.80	-0.10
1808	0.77	-0.24	1632	0.85	0.11	1436	0.77	-0.28	1215	0.78	-0.22
1806	0.80	-0.13	1630	0.79	-0.17	1433	0.76	-0.31	1212	0.79	-0.16
1804	0.77	-0.26	1628	0.80	-0.13	1431	0.77	-0.28	1209	0.89	0.27
1801	0.79	-0.17	1625	0.74	-0.39	1428	0.76	-0.31	1206	0.92	0.43
1799	0.82	-0.04	1623	0.82	-0.04	1426	0.74	-0.42	1204	0.86	0.16
1797	0.81	-0.10	1621	0.81	-0.09	1423	0.70	-0.59	1201	0.85	0.11
1795	0.79	-0.16	1618	0.78	-0.22	1421	0.69	-0.62	1198	0.80	-0.13
1793	0.75	-0.37	1616	0.78	-0.24	1418	0.70	-0.60	1195	0.77	-0.26
1791	0.73	-0.45	1613	0.83	0.02	1415	0.67	-0.71	1192	0.82	-0.02
1789	0.75	-0.38	1611	0.86	0.13	1413	0.68	-0.69	1190	0.94	0.51
1787	0.77	-0.25	1609	0.84	0.04	1410	0.69	-0.61	1187	0.95	0.59
1785	0.77	-0.27	1606	0.80	-0.12	1408	0.69	-0.62	1184	0.96	0.63
1783	0.77	-0.28	1604	0.85	0.09	1405	0.68	-0.68	1181	0.96	0.62
1781	0.88	0.22	1602	0.80	-0.12	1402	0.65	-0.80	1179	0.95	0.58
1779	0.85	0.10	1599	0.83	0.00	1400	0.62	-0.96	1176	0.96	0.60
1776	0.84	0.05	1597	0.82	-0.04	1397	0.61	-0.98	1173	0.97	0.64
1774	0.82	-0.04	1595	0.78	-0.24	1395	0.66	-0.79	1170	1.01	0.86
1772	0.90	0.35	1592	0.78	-0.23	1392	0.63	-0.92	1167	0.98	0.71
1770	0.88	0.25	1590	0.78	-0.24	1389	0.65	-0.82	1165	1.03	0.94
1768	0.87	0.21	1587	0.72	-0.49	1387	0.65	-0.83	1162	1.01	0.83
1766	0.87	0.19	1585	0.70	-0.58	1384	0.65	-0.82	1159	0.99	0.75

Table S5: Continued

Age AD/BC	Ca/Si	NAO_{TRD}	Age AD/BC	Ca/Si	NAO_{TRD}	Age AD/BC	Ca/Si	NAO_{TRD}	Age AD/BC	Ca/Si	NAO_{TRD}
1156	0.95	0.59	921	0.70	-0.61	683	0.79	-0.18	435	0.91	0.38
1153	0.92	0.42	918	0.69	-0.62	680	0.78	-0.24	432	0.88	0.24
1151	0.93	0.45	915	0.66	-0.75	677	0.78	-0.20	429	0.91	0.38
1148	0.88	0.23	912	0.70	-0.59	674	0.82	-0.04	426	0.90	0.31
1145	0.86	0.15	909	0.67	-0.73	671	0.78	-0.23	423	0.96	0.59
1142	0.90	0.35	906	0.66	-0.78	668	0.79	-0.18	420	0.96	0.62
1139	0.92	0.45	903	0.65	-0.81	665	0.76	-0.31	417	0.95	0.58
1137	0.89	0.27	900	0.65	-0.82	662	0.77	-0.29	414	0.88	0.24
1134	0.88	0.26	897	0.65	-0.80	659	0.77	-0.27	411	0.88	0.24
1131	0.89	0.31	895	0.63	-0.89	656	0.76	-0.30	408	0.88	0.24
1128	0.89	0.27	892	0.59	-1.10	653	0.76	-0.32	405	0.87	0.19
1125	0.93	0.46	889	0.56	-1.23	650	0.76	-0.33	402	0.90	0.31
1122	0.96	0.60	886	0.61	-0.99	647	0.75	-0.37	399	0.86	0.14
1120	0.92	0.43	883	0.64	-0.87	644	0.71	-0.56	396	0.83	0.02
1117	0.89	0.30	880	0.60	-1.03	641	0.70	-0.60	393	0.85	0.10
1114	0.88	0.26	877	0.55	-1.26	638	0.69	-0.61	390	0.89	0.27
1111	0.91	0.40	874	0.54	-1.33	635	0.71	-0.52	387	0.88	0.23
1108	0.94	0.50	871	0.52	-1.44	632	0.71	-0.54	384	0.90	0.34
1106	0.88	0.22	868	0.55	-1.28	629	0.68	-0.69	381	0.91	0.37
1103	0.78	-0.22	865	0.53	-1.35	626	0.66	-0.76	378	0.92	0.41
1100	0.80	-0.15	862	0.60	-1.07	623	0.66	-0.76	375	0.92	0.43
1097	0.85	0.09	859	0.67	-0.71	620	0.68	-0.70	371	0.98	0.68
1094	0.84	0.04	856	0.66	-0.75	617	0.67	-0.71	368	1.01	0.85
1091	0.83	0.03	853	0.67	-0.71	614	0.71	-0.53	365	0.94	0.50
1088	0.83	0.03	850	0.70	-0.58	611	0.76	-0.29	362	0.99	0.77
1086	0.90	0.31	847	1.01	0.83	608	0.69	-0.63	359	0.95	0.56
1083	0.85	0.13	844	1.04	0.99	605	0.72	-0.51	356	0.97	0.67
1080	0.94	0.54	841	1.00	0.82	602	0.67	-0.70	353	0.99	0.74
1077	0.91	0.38	838	1.12	1.37	599	0.68	-0.68	350	1.00	0.80
1074	0.90	0.34	835	1.06	1.08	596	0.73	-0.45	347	0.98	0.69
1071	0.87	0.21	833	1.09	1.20	593	0.73	-0.47	344	0.93	0.48
1069	0.85	0.09	830	1.05	1.00	590	0.69	-0.65	341	0.93	0.46
1066	0.86	0.16	827	1.02	0.88	587	0.71	-0.54	338	0.91	0.38
1063	0.87	0.20	824	1.02	0.90	584	0.81	-0.10	335	0.75	-0.34
1060	0.89	0.30	821	0.91	0.36	581	0.72	-0.50	332	1.04	1.00
1057	0.86	0.16	818	0.95	0.57	578	0.75	-0.35	329	1.04	1.00
1054	0.84	0.06	815	1.01	0.82	575	0.75	-0.38	326	1.02	0.89
1051	0.83	0.02	812	1.04	0.97	572	0.75	-0.33	323	1.02	0.87
1048	0.84	0.05	809	1.06	1.09	569	0.77	-0.26	320	1.03	0.92
1046	0.85	0.10	806	1.07	1.11	566	0.70	-0.58	317	1.00	0.78
1043	0.83	0.01	803	1.11	1.29	563	0.74	-0.42	314	0.94	0.52
1040	0.83	-0.01	800	1.07	1.14	559	0.71	-0.52	311	0.95	0.57
1037	0.82	-0.06	797	1.01	0.83	556	0.71	-0.55	308	0.95	0.55
1034	0.86	0.15	794	1.00	0.79	553	0.72	-0.50	305	0.92	0.41
1031	0.82	-0.03	791	1.01	0.84	550	0.74	-0.39	302	0.91	0.38
1028	0.93	0.46	788	1.02	0.88	547	0.75	-0.34	299	0.93	0.46
1026	0.82	-0.03	785	1.02	0.87	544	0.71	-0.55	296	0.91	0.39
1023	0.90	0.31	782	0.97	0.66	541	0.80	-0.13	293	0.88	0.26
1020	0.84	0.07	779	1.00	0.81	538	0.73	-0.45	290	0.89	0.27
1017	0.84	0.06	776	0.98	0.70	535	0.76	-0.33	287	0.86	0.15
1014	0.83	0.00	773	0.93	0.49	532	0.76	-0.30	284	0.86	0.16
1011	0.82	-0.04	770	0.97	0.65	529	0.87	0.20	281	0.84	0.07
1008	0.84	0.06	767	0.96	0.62	526	0.95	0.54	278	0.84	0.06
1005	0.89	0.29	764	0.96	0.60	523	0.94	0.53	275	0.86	0.16
1002	0.86	0.16	761	0.93	0.48	520	0.94	0.51	271	0.86	0.14
1000	0.88	0.26	758	0.94	0.51	517	0.93	0.48	268	0.78	-0.24
997	0.91	0.36	755	0.95	0.59	514	0.87	0.19	265	0.78	-0.21
991	1.01	0.83	752	0.97	0.66	511	0.85	0.11	262	0.75	-0.34
988	0.81	-0.07	749	0.98	0.70	508	0.87	0.20	259	0.78	-0.23
982	0.86	0.13	746	0.86	0.16	505	0.92	0.41	256	0.77	-0.26
979	0.92	0.41	743	0.86	0.13	502	0.93	0.47	253	0.78	-0.21
976	0.84	0.07	740	0.84	0.08	499	0.93	0.47	250	0.77	-0.28
973	0.80	-0.12	737	0.89	0.30	496	0.95	0.56	247	0.84	0.05
971	0.80	-0.14	734	0.81	-0.08	493	0.95	0.57	244	0.89	0.31
968	0.81	-0.07	731	0.86	0.15	490	0.92	0.44	241	0.83	0.02
965	0.81	-0.10	728	0.85	0.11	487	0.95	0.56	238	0.84	0.08
962	0.85	0.10	725	0.88	0.25	484	0.94	0.53	235	0.84	0.04
959	0.85	0.10	722	0.89	0.27	481	0.92	0.43	232	0.86	0.15
956	0.86	0.14	719	0.88	0.22	478	0.90	0.33	229	0.85	0.13
953	0.84	0.08	716	0.85	0.10	475	0.90	0.34	226	0.89	0.27
950	0.91	0.37	713	0.85	0.09	472	0.88	0.24	223	0.85	0.10
947	0.79	-0.17	710	0.88	0.22	469	0.85	0.11	220	0.85	0.10
944	0.79	-0.19	707	0.87	0.21	466	0.84	0.05	217	0.85	0.09
941	0.77	-0.25	704	0.87	0.20	463	0.87	0.21	214	0.88	0.22
938	0.76	-0.31	701	0.89	0.30	453	0.92	0.43	211	0.86	0.16
936	0.78	-0.21	698	0.87	0.19	450	0.88	0.23	208	0.86	0.14
933	0.79	-0.15	695	0.88	0.26	447	0.94	0.52	205	0.87	0.18
930	0.75	-0.36	692	0.83	0.02	444	0.94	0.53	202	0.86	0.16
927	0.74	-0.41	689	0.80	-0.14	441	0.93	0.47	199	0.87	0.19
924	0.70	-0.61	686	0.79	-0.15	438	0.90	0.32	196	0.85	0.11

Table S5: Continued

Age AD/BC	Ca/Si	NAO_{TRD}	Age AD/BC	Ca/Si	NAO_{TRD}	Age AD/BC	Ca/Si	NAO_{TRD}	Age AD/BC	Ca/Si	NAO_{TRD}
193	0.84	0.07	-46	0.66	-0.77	-277	0.75	-0.35	-497	0.81	-0.08
190	0.82	-0.05	-49	0.64	-0.88	-280	0.75	-0.38	-500	0.80	-0.14
187	0.81	-0.06	-52	0.65	-0.81	-283	0.68	-0.66	-502	0.88	0.25
184	0.77	-0.26	-55	0.65	-0.83	-285	0.66	-0.78	-505	0.85	0.08
181	0.74	-0.39	-57	0.63	-0.89	-288	0.65	-0.82	-507	0.82	-0.06
178	0.73	-0.45	-60	0.63	-0.89	-291	0.71	-0.53	-510	0.81	-0.07
175	0.71	-0.52	-63	0.62	-0.98	-294	0.73	-0.44	-513	0.85	0.09
172	0.73	-0.44	-66	0.62	-0.97	-297	0.71	-0.52	-515	0.82	-0.01
169	0.72	-0.49	-69	0.62	-0.95	-299	0.71	-0.56	-518	0.85	0.09
166	0.74	-0.38	-72	0.62	-0.97	-302	0.72	-0.50	-521	0.77	-0.25
163	0.74	-0.41	-75	0.61	-0.99	-305	0.72	-0.49	-523	0.74	-0.40
160	0.73	-0.46	-78	0.62	-0.97	-308	0.73	-0.44	-526	0.79	-0.16
157	0.74	-0.42	-81	0.62	-0.98	-311	0.76	-0.33	-529	0.80	-0.15
154	0.76	-0.29	-84	0.66	-0.79	-314	0.73	-0.43	-531	0.86	0.14
151	0.75	-0.34	-87	0.73	-0.44	-316	0.72	-0.50	-534	0.86	0.14
148	0.69	-0.63	-90	0.74	-0.40	-319	0.73	-0.47	-537	0.86	0.16
145	0.70	-0.61	-93	0.76	-0.31	-322	0.72	-0.48	-539	0.85	0.08
142	0.66	-0.75	-96	0.77	-0.26	-325	0.63	-0.92	-542	0.84	0.07
139	0.70	-0.59	-98	0.71	-0.54	-328	0.60	-1.07	-544	0.77	-0.25
136	0.73	-0.46	-101	0.68	-0.68	-330	0.58	-1.13	-547	0.72	-0.50
133	0.71	-0.52	-104	0.69	-0.64	-333	0.58	-1.13	-550	0.69	-0.61
130	0.71	-0.56	-107	0.65	-0.82	-336	0.57	-1.18	-552	0.66	-0.75
127	0.70	-0.58	-110	0.69	-0.62	-339	0.56	-1.23	-555	0.68	-0.66
124	0.74	-0.41	-113	0.86	0.15	-341	0.58	-1.16	-557	0.71	-0.56
121	0.74	-0.42	-116	0.85	0.10	-344	0.57	-1.17	-560	0.68	-0.68
118	0.73	-0.44	-119	0.87	0.19	-347	0.57	-1.18	-563	0.68	-0.69
115	0.75	-0.38	-122	0.83	0.00	-350	0.59	-1.10	-565	0.69	-0.63
112	0.75	-0.37	-125	0.86	0.13	-353	0.65	-0.80	-568	0.67	-0.75
109	0.74	-0.42	-128	0.84	0.06	-355	0.62	-0.97	-570	0.69	-0.62
106	0.73	-0.46	-131	0.81	-0.09	-358	0.63	-0.91	-573	0.68	-0.66
103	0.76	-0.31	-133	0.80	-0.11	-361	0.63	-0.89	-576	0.69	-0.61
100	0.79	-0.19	-136	0.85	0.12	-364	0.61	-0.99	-578	0.67	-0.74
97	0.79	-0.18	-139	0.83	-0.01	-366	0.64	-0.88	-581	0.71	-0.55
94	0.74	-0.40	-142	0.71	-0.54	-369	0.63	-0.92	-583	0.75	-0.36
91	0.74	-0.42	-145	0.73	-0.47	-372	0.65	-0.81	-586	0.76	-0.32
88	0.78	-0.21	-148	1.05	1.04	-375	0.67	-0.74	-589	0.67	-0.73
85	0.82	-0.04	-151	0.71	-0.56	-378	0.65	-0.81	-591	0.67	-0.73
82	0.83	0.02	-154	0.77	-0.27	-380	0.62	-0.93	-594	0.70	-0.60
79	0.86	0.15	-157	0.77	-0.26	-383	0.62	-0.97	-596	0.68	-0.68
76	0.86	0.15	-160	0.81	-0.08	-386	0.55	-1.28	-599	0.68	-0.69
73	0.85	0.10	-162	0.79	-0.16	-389	0.63	-0.93	-601	0.68	-0.70
70	0.87	0.19	-165	0.84	0.06	-391	0.64	-0.87	-604	0.65	-0.83
67	0.83	0.00	-168	0.84	0.04	-394	0.62	-0.94	-607	0.67	-0.74
64	0.83	0.02	-171	0.79	-0.18	-397	0.61	-0.98	-609	0.69	-0.64
61	0.82	-0.05	-174	0.84	0.04	-400	0.64	-0.87	-612	0.64	-0.84
58	0.82	-0.02	-177	0.91	0.40	-402	0.64	-0.84	-614	0.64	-0.87
55	0.86	0.16	-180	0.88	0.22	-405	0.62	-0.96	-617	0.67	-0.75
52	0.84	0.07	-183	0.84	0.08	-408	0.61	-1.02	-619	0.65	-0.83
49	0.88	0.23	-186	0.85	0.12	-410	0.62	-0.93	-622	0.63	-0.91
46	0.88	0.26	-188	0.86	0.14	-413	0.61	-0.98	-624	0.80	-0.14
43	0.85	0.08	-191	0.85	0.12	-416	0.57	-1.17	-627	0.74	-0.41
40	0.86	0.15	-194	0.89	0.30	-419	0.63	-0.92	-629	0.67	-0.73
37	0.85	0.12	-197	0.97	0.64	-421	0.65	-0.80	-632	0.64	-0.86
34	0.84	0.04	-200	0.91	0.39	-424	0.57	-1.18	-635	0.64	-0.85
31	0.93	0.49	-203	0.83	0.00	-427	0.54	-1.34	-637	0.62	-0.96
28	0.85	0.09	-206	0.83	-0.01	-430	0.74	-0.42	-640	0.59	-1.11
25	0.81	-0.08	-209	0.85	0.12	-432	0.76	-0.31	-642	0.60	-1.06
22	0.83	0.01	-211	0.80	-0.14	-435	0.74	-0.41	-645	0.60	-1.06
19	0.80	-0.12	-214	0.82	-0.04	-438	0.76	-0.30	-647	0.62	-0.93
16	0.76	-0.30	-217	0.83	-0.01	-440	0.75	-0.37	-650	0.62	-0.96
13	0.81	-0.07	-220	0.83	0.01	-443	0.79	-0.19	-652	0.62	-0.95
10	0.76	-0.31	-223	0.86	0.13	-446	0.76	-0.31	-655	0.60	-1.05
8	0.75	-0.37	-226	0.86	0.15	-449	0.79	-0.17	-657	0.65	-0.84
5	0.78	-0.23	-229	0.86	0.14	-451	0.81	-0.09	-660	0.65	-0.83
2	0.78	-0.24	-231	0.80	-0.11	-454	0.80	-0.14	-662	0.62	-0.93
-1	0.78	-0.24	-234	0.80	-0.11	-457	0.78	-0.20	-665	0.59	-1.07
-4	0.81	-0.09	-237	0.84	0.05	-459	0.77	-0.26	-667	0.64	-0.88
-7	0.78	-0.20	-240	0.82	-0.01	-462	0.78	-0.22	-670	0.60	-1.02
-10	0.78	-0.21	-243	0.81	-0.06	-465	0.79	-0.16	-672	0.62	-0.94
-13	0.75	-0.37	-246	0.79	-0.17	-467	0.79	-0.17	-675	0.64	-0.86
-16	0.78	-0.22	-249	0.82	-0.01	-470	0.84	0.05	-677	0.62	-0.97
-19	0.76	-0.29	-251	0.78	-0.22	-473	0.86	0.14	-680	0.59	-1.11
-22	0.72	-0.49	-254	0.75	-0.36	-475	0.95	0.55	-682	0.59	-1.11
-25	0.74	-0.42	-257	0.76	-0.30	-478	0.81	-0.09	-684	0.61	-1.02
-28	0.79	-0.17	-260	0.74	-0.42	-481	0.83	0.02	-687	0.58	-1.15
-31	0.72	-0.49	-263	0.75	-0.34	-484	0.81	-0.06	-689	0.61	-1.01
-34	0.71	-0.55	-266	0.79	-0.18	-486	0.81	-0.10	-692	0.64	-0.87
-37	0.71	-0.52	-268	0.80	-0.12	-489	0.79	-0.18	-694	0.60	-1.04
-40	0.72	-0.50	-271	0.79	-0.18	-492	0.74	-0.40	-697	0.62	-0.96
-43	0.71	-0.53	-274	0.75	-0.34	-494	0.78	-0.24	-699	0.66	-0.77

Table S5: Continued

Age AD/BC	Ca/Si	NAO_{TRD}
-702	0.64	-0.85
-704	0.65	-0.83
-707	0.69	-0.65
-709	0.74	-0.38
-711	0.70	-0.58
-714	0.73	-0.47
-716	0.74	-0.39
-719	0.77	-0.28
-721	0.72	-0.49
-724	0.69	-0.63
-726	0.69	-0.63
-728	0.68	-0.69
-731	0.68	-0.70
-733	0.63	-0.92
-736	0.70	-0.57
-738	0.70	-0.59
-741	0.73	-0.46
-743	0.73	-0.43
-745	0.72	-0.51
-748	0.71	-0.52
-750	0.69	-0.65
-753	0.68	-0.69
-755	0.70	-0.60
-757	0.70	-0.60
-760	0.71	-0.55
-762	0.76	-0.32
-764	0.73	-0.43
-767	0.75	-0.35
-769	0.75	-0.36
-772	0.77	-0.26
-774	0.73	-0.44
-776	0.73	-0.44
-779	0.77	-0.26
-781	0.75	-0.36
-783	0.81	-0.08
-786	0.74	-0.42
-788	0.72	-0.51
-790	0.71	-0.54
-793	0.72	-0.49
-795	0.75	-0.34